

Hydrogen Production by Steam Reforming of Methanol over a Ag/ZnO One Dimensional Catalyst

R. Pérez-Hernández, A. Gutiérrez-Martínez, A. Mayoral, F. Leonard Deepak, Ma. E. Fernández-García, G. Mondragón-Galicia, M. Miki, M. Jose-Yacaman.

Abstract

One dimensional (1-D) and three dimensional (3-D) ZnO were growth by a hydrothermal method. ZnO 1-D was employed as a support for silver nanoparticles in order to design a new catalyst and used on the steam reforming of methanol (SRM) reaction for H₂ production. The catalytic activity of the Ag/ZnO sample with low content of Ag showed better performance on the SRM reaction than on high silver loading catalyst. So, the sample with small Ag particle size showed best performance in methanol conversion than catalyst with big Ag particle size, this finding could be attributed to the high ZnO/Ag ratio. According to results of SEM and TEM techniques the catalytic activity: methanol conversion, H₂ and low CO production observed on the Ag/ZnO 1-D catalyst occurs in the edge sites rather than the rim sites. The role of Ag is to accept the hydrogen to be released to the gas phase. In addition, the 1.5Ag/ZnO 1-D catalyst showed good stability during the reaction.

Keywords: Steam reforming of methanol, Ag/ZnO one dimensional catalyst, Ag dispersion, ZnO rods and nanostars; ZnO nanostructures; SEM; TEM; edge/rim sites.

Introduction

The technologies for the production of high-quality transportation fuels from non-petroleum hydrocarbon resources have attracted considerable attention by scientists

and chemical companies in accordance with the recent environmental demands and the decrease of fossil energy reserves. The fuel cell technology offers the potential to reduce the consumption of energy resources and the emissions of environmental pollutants from automobiles and electric power plants. In particular, polymer electrolyte fuel cell (PEFC) systems using hydrogen as an energy source, have attracted much attention due to their low operating temperature [1]. Conventional hydrogen production methods use gasoline or natural gas reforming. However, from the different feed stock fuels available, alcohols are very promising candidates because they are easily decomposed in the presence of water and generate a hydrogen-rich mixture at relatively low temperatures.

Methanol has been identified as a highly suitable liquid fuel for H₂ production, because of its high hydrogen/carbon ratio which favors energetically the steam reforming of methanol (SRM), as well as, the absence of carbon-carbon bonds which reduces soot formation, which otherwise may lead to deactivation of the catalyst [2; 3] and ease of handling. Oxidative Steam Reforming of Methanol (OSRM) and Steam Reforming of Methanol (SRM) for hydrogen production on Cu, Ni, Au and Pd supported on CeO₂, ZrO₂ and Al₂O₃ has been extensively studied in recent years [4; 5; 6; 7; 8; 9; 10; 11]. Iwasa et al. [12] reported that ZnO base-catalysts have exceptionally high activity and selectivity to CO₂ and H₂ on the steam reforming of methanol and methanol synthesis [13] with low selectivity toward methane [14; 15]. Copper zinc oxide catalysts are important commercially in the conversion or preparation of synthetic gas [16]. Although several new systems were proposed for different reactions with ZnO-base catalysts, no decisive novelty appeared in the last years. In this context, new highly

active and selective catalysts are necessary in order to advance the industry of the high-quality transportation fuels. This is particularly important in the case of one-dimensional (1D) structures such as rods, whose large surface to-volume ratio and dimensionality make them especially sensitive to surface-mediated interactions which in turn, impact the properties and performance of these materials to be used as catalytic materials. Therefore, controlling the synthetic process in order to select and control the presence of specific materials is a challenge and it is a very important subject of research around the world. For this reason we prepared Zinc oxide (ZnO) 1D rods and, used them as a support for silver nanoparticles. Ag/ZnO nanocomposites have attracted much attention because Ag is an extremely attractive noble metal to be investigated at the nanoscale due to its significant catalytic activity and environment remediation of contaminants and destruction of microorganisms [17; 18].

The objective of this article thus aims at introducing design of new class of materials for use as a catalytic material for hydrogen production. For this objective we report a hydrothermal method for the synthesis of ZnO nanostars and 1-D rods to support silver nanoparticles as an active phase. The growth morphology of these nanostructures especially the 1-D catalyst was studied in detail using electron microscopy techniques, and their catalytic activity was studied in the steam reforming of methanol for H₂ production.

Experimental Method

Synthesis of the ZnO nanostructures: All reagents including zinc nitrate (Zn(NO₃)₂•6H₂O) and sodium hydroxide (NaOH), were analytical grade purchased from Aldrich and used as received. For the production of the ZnO 3D stars, 20 mL of 0.05 M

NaOH solution was added to 10 mL of deionized water under magnetic stirring, then, 20 mL of 0.01 M $\text{Zn}(\text{NO}_3)_2 \cdot 6\text{H}_2\text{O}$ solution was added drop wise to complete the precipitation at 19 °C. The ZnO 1D rods were synthesized using the method reported previously [19; 20; 21]. 8 mL of 4 M NaOH solution was added to 32 mL of deionized water under magnetic stirring, followed by the drop wise addition of 16 mL of 0.2 M $\text{Zn}(\text{NO}_3)_2 \cdot 6\text{H}_2\text{O}$ to complete the precipitation. The solution was stirred for 10 min and, then the mixture was transferred into a Teflon-lined stainless steel autoclave with a capacity of 125 mL. The autoclave was sealed and kept under heating for 6 h. After the reaction was completed, the mixture was cooled to room temperature and the white powder obtained was separated from the solution by centrifugation. The as-obtained ZnO powder was washed several times with deionized water and ethanol and dried at 80 °C for 24 h.

Catalysts preparation (Ag/1D-ZnO):

The synthesized ZnO 1D rods were impregnated with an aqueous solution of AgNO_3 at an appropriate concentration to yield 1.5 and 5 wt % of Ag in the catalysts. The samples were the dried at 100°C for 1h and calcined at 400 °C for 2h in static air and finally reduced with a H_2 stream at 400 °C for 1h before further characterization. The labeling of different catalysts will be referred as xAg/ZnO, where x = 1.5 and 5 wt % of metal on the catalysts respectively.

Characterization:

The morphology of the rods was analyzed by Scanning Electron Microscopy (SEM) which was performed in a FEG Hitachi S-5500 ultra high resolution electron

microscope (0.4 nm at 30kV) with a BF/DF Duo-STEM detector. Transmission electron microscopy (TEM), selected area electron diffraction (SAED) and weak beam dark field (WBDF) analysis were performed using a Philips Tecnai G2, 200Kv, TEM equipped with Schottky-type field emission gun, ultra-high resolution pole piece ($C_s=0.5$ mm), and a scanning transmission electron microscope (STEM) unit with high angle annular dark field (HAADF) detector operating at 200 kV. X-ray diffraction (XRD) powder patterns were recorded in a Siemens D-5000 diffractometer, using Cu K α ($\lambda=0.15406$ nm). The ZnO model was built using the program Cerius2 that allows the geometric optimization of the model with classical mechanical simulation. The calculus is based on classical mechanical that uses universal potential [22; 23; 24] to corroborate the experimental results. The transmission electron microscope parameters used to carry out the simulation process correspond to the JEOL 2010 microscope with an acceleration voltage of 200 kV, a spherical aberration coefficient of 0.5 mm, a beam divergence half-angle of 0.6 mrad and Scherzer resolution of 0.17 nm.

The method to measure the total surface area and TPR was reported previously [4; 5; 11; 24; 25; 26; 27]. The steady-state activity in the SRM reaction was performed in a conventional fixed-bed flow reactor (8 mm i.d.) using 0.1 g of the catalyst in a temperature range from 250 to 475 °C with steps of 25 °C with 7 h of stabilization time at each temperature and atmospheric pressure on an automatic multitask unit RIG-100 from ISR INC. The catalyst was first activated in a stream of H₂ (60 ml/min) from room temperature to 400 °C with a heating rate of 10°C/min and held at this temperature for 1h. A thermocouple in contact with the catalytic bed allowed the control of the temperature inside the catalyst was used. The sample was brought up to the reaction

temperature in He and the reaction mixture was introduced. For the SRM reaction, He (50 ml/min, GHSV= 30,000 h⁻¹ based on the total flow) was added by means of two mass flow controller (RIG- 100) and bubbled through a tank containing water and the other methanol, the partial pressure of CH₃OH and H₂O was 75 and 12.75 Torr respectively. The effluent gas of the reactor was analyzed by gas-chromatography (Gow-Mac 580 instrument) equipped with a two columns system (molecular sieve 5 Å and Porapack Q columns), double injector controlled by Clarity software V.2.6.04.402 and TCD. The first column was used to separate the gaseous products such as H₂, O₂, CH₄ and CO. The second column was used to separate water, methanol, methyl formate (MF) and CO₂. The GC analysis was performed in isothermal conditions (oven temperature = 110 °C). The spent 1.5Ag/ZnO catalyst was tested again in a second cycle of catalytic activity. So at the end of the reaction (400 °C) the catalyst was cleaned with He for 30 min. Then the sample was brought up to the reaction temperature in He and the reaction mixture was introduced and the catalytic activity for the second cycle was determined. The following equation was used to determine the methanol conversion:

$$X(\%) = \frac{C_{in} - C_{out}}{C_{in}} * 100 \quad (1)$$

The subscripts in and out indicate the inlet and the outlet concentrations of the reactants.

Results and Discussions

ZnO with 1D and 3D morphologies were growth modifying the concentration of the precursors during the synthesis. A typical SEM image of the ZnO 3D microstructure with star-like morphology is shown in Fig. 1a. It showed on the middle of the axis, six relatively shorter ($0.75\ \mu\text{m}$) cones. Figure 1b showed the TEM results of the ZnO three-dimensional nanostars.

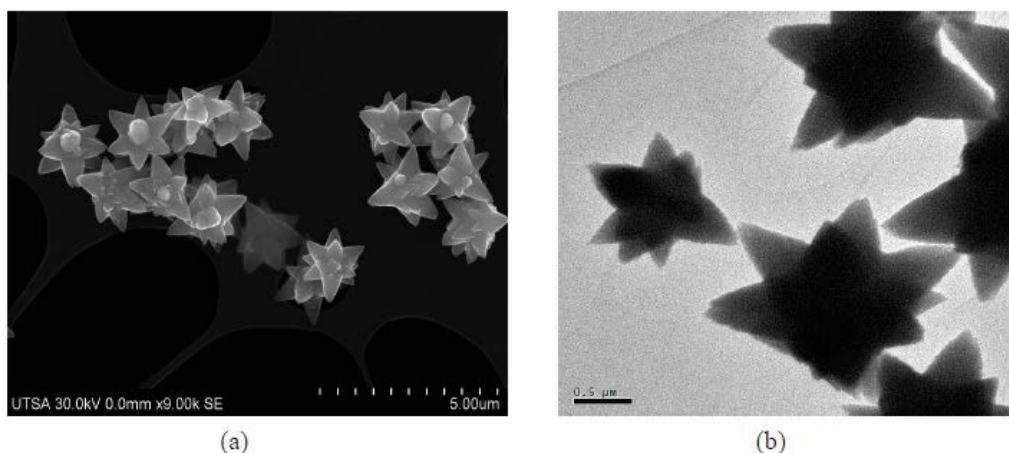


Figure 1. (a) Typical SEM image of the 3D ZnO structure. (b) Low magnification TEM images of the nanostars

It was reported in the literature that the formation mechanism of the 3D structure involves the enhancing effect on the growth of ZnO $[0\ 0\ 01]$ direction [21] and the secondary nucleation process [28]. Feng et al. [28] found that in the early growth stage of the ZnO 3D structures; nut-shape crystals were formed which were constructed by two hexagonal cones. Gao et al. [29] suggested that employing ethylene diamine was the way to obtained nanostars. They proposed that the ethylene diamine was hydrolyzed and formed ethylene diamine- H_2 complex network. Thus, by the coulomb interaction, ethylenediamine- H_2 molecules were adsorbed on the negative polar planes (i.e., (1011) , (1010) and (1011) planes) retarding the growth rate of these planes.

Therefore, the concentration of ethylene diamine in the precursor has a significant effect on the morphology of ZnO crystals. When the concentration of ethylene diamine was high enough, ethylenediamine- H_2 molecules covered all the side surfaces of the ZnO crystal, enhancing the growth along the (0002) plane greatly and resulting in the formation of rods with uniform diameters and high aspect ratios. However, when the concentration of ethylene diamine was relatively low, there were not enough ethylenediamine- H_2 molecules to cover all the side surfaces of ZnO crystal. So, both the impeding effect of ethylene diamine on the crystal growth and the Ostwald ripening process took place, resulting in the formation of petal crystals with the obvious tapering feature. In our case we did not use any other nucleation-control reagent to obtain the six-fold symmetry of the ZnO 3D structures. Thus, the concentration of the $[OH^-]$ and $[Zn^{2+}]$ in the solution is the most important parameter to obtain these kind of structures. In addition, we observed more side-branches on the ZnO nanostars, which may be formed by prolonging the growing time although they preserved some six-fold symmetry. On the other hand, the lower concentration of the $[OH^-]$ and $[Zn^{2+}]$ in the solution, induced that the clusters did not interact between them due to the low presence of the cations and anions in the suspension, causing that the 3D structure did not grow toward the rods.

Further increasing of the concentration of the $[OH^-]$ and $[Zn^{2+}]$ resulted in the formation of cactus-like ZnO nanostructures. Secondary growth produced agave-like crystals from new crystal growth on the edges. The SEM images (Figure 2a) reveals that the flowers consisted of nanoneedles with lengths of about 7 μm and diameters of about 900 nm and other near to 150 nm. Each flower has a central part as a common

growth point for all of the constituent nanoneedles. Inset in Figure 2a, showed that the ZnO 1D crystal obtained by the hydrothermal method belongs to the hexagonal crystal system. However, when the sample was seen in transversal section (Figure 2b) the top of the rod showed a sharp tip. The reason for the alignment of the ZnO structure is due to the matching lattice structure through the polar nature of the ZnO surface [19]. Initially, the ZnO crystalline grains mainly grow along the $\langle 01\bar{1}0 \rangle$ direction due to epitaxy. However, as a result of the polar characteristic of the ZnO, the growth along the $\langle 0001 \rangle$ direction has a gradual increasing velocity [30]. ZnO surface is either positively or negatively charged. In either case the surface would attract ions of opposite charges (OH^- or Zn^{2+}) to it. This new surface covered with ions, would attract more ions with opposite charges to cover the following surface and thereby react to form ZnO. As in most cases, the surfaces of the metal oxide nanoparticles formed in hydrothermal conditions were terminated by hydroxyl groups [31]. The increase in the concentration of the precursor solution enhance the amount of both zinc cations (Zn^{2+} ions) and hydroxyl anions (OH^- ions) which would react with each other in order to form stable $\text{Zn}(\text{OH})_2$ complexes (growth units of ZnO rods).

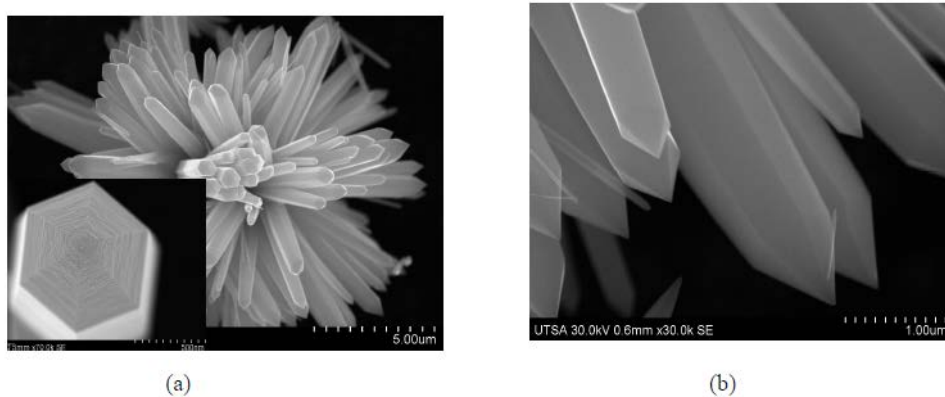


Figure 2. a) SEM image of the 1D ZnO rods. Inset Figure in (a), showed a top view of the rod.
b) Transversal section of the rods showed a sharp tip.

During the crystallization of ZnO, OH⁻ ions contained at the surface of ZnO crystal have a shielding effect on the growth of ZnO rods [21, 32]. We noted that the average diameter of ZnO rods proportionally increased as the concentration of the precursor solution was increased. Due to the higher amount of the growing units of ZnO, the diameters of ZnO rods swelled, effect attributed to the radial growth along the <0110> direction [20]. The formation of hexagonal prism and pyramid like ZnO crystals is attributed to the difference in the growth velocities of the various crystal facets. The growth velocities of ZnO under hydrothermal conditions along the different directions has been already reported to be (0001) > (1011) > (1010) [19; 32; 33]. On the other hand, we found that the growth time and the basicity of the solution played a crucial role in order to obtain the 3D structures or the 1D rods.

Detailed structural characterization of the zinc oxide rod before Ag impregnation was performed by

TEM analysis. Figure 3a shows a low magnification TEM image of a typical ZnO rods obtained in this work, the diameter of this rod was about 150 nm. All of these rods terminate in a triangular truncated phase which has a diameter of 30 nm. Inset in Figure 3a shows the SAEDP electron diffraction pattern in [1 2 1 0] direction of the entire wire in which we can observe forbidden spots along the planes {0001}. In addition, the SAEDP revealed a single crystal structure along the entire rod which was also confirmed with HRTEM images indicating that it grows free of defects. The high resolution image (Figure 3b) suggests that the ZnO 1D grew along the c axis, which corresponds to the [0001] direction.

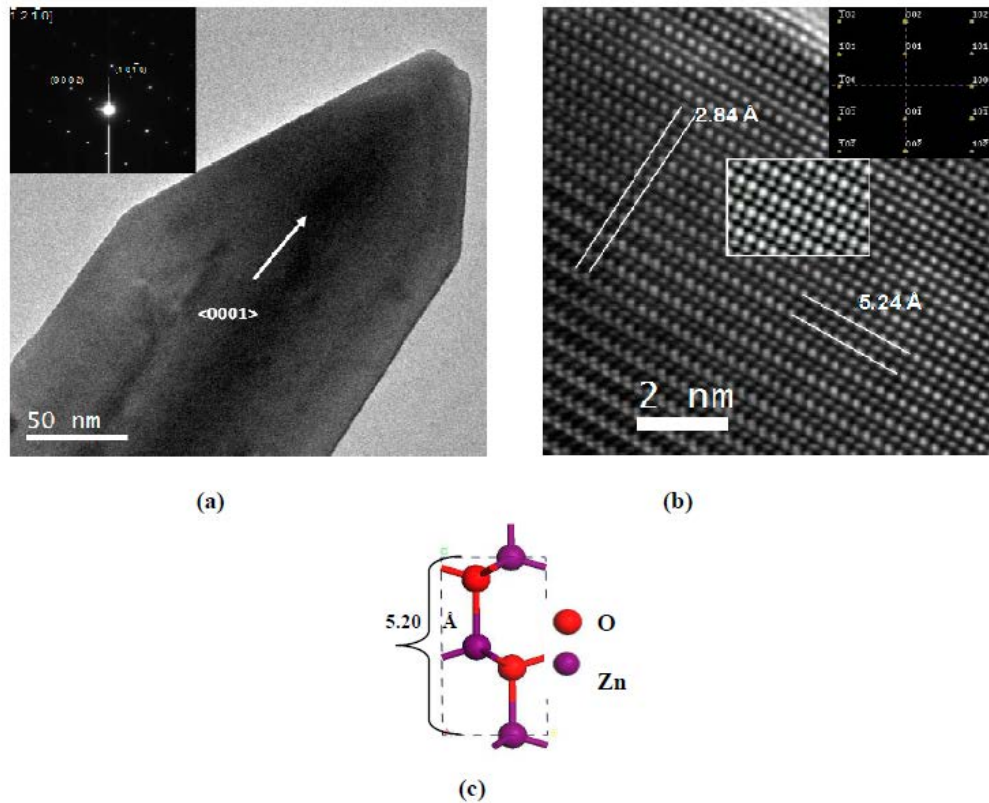


Figure 3. a) Low magnification TEM images of one of the rods that growth along the [0001] directions. Inset image in (a) showed the experimental electron diffraction pattern in the $[\bar{1}2\bar{1}0]$ direction. b) HRTEM images of the rod showed in (a). Inset the HRTEM images simulated ZnO structure in the [010] direction which corresponds to $[\bar{1}2\bar{1}0]$ orientation where the forbidden points appear, both images match. c) Unit cell of ZnO model (Zn-purple and O-red atoms).

The lattice planes were identified (Figure 3b) and the experimental values obtained for $d_{(0001)} \approx 5.24 \text{ \AA}$ and $d_{(10\bar{1}0)} \approx 2.84 \text{ \AA}$ were very close to the theoretically predicted. The different contrast observed in Figure 3b between each layer of atoms is attributed to the atomic arrays of the direction observation $[\bar{1}2\bar{1}0]$ and to the defocus of the image according to the thickness of the sample. In other words, each layer of atoms lay on different planes as it is shown in the ZnO model, Figure 3c. In which, the central Zn atom is situated exactly in the middle of another two Zn atoms but in a different plane. This affirmation was confirmed with the simulation of the ZnO model (inset image, Figure 3b) in which experimental and simulated images match. On the other

hand, the experimental SAEDP pattern showed two extra spots which were not observed on the simulated one. We believed that the appearance of those forbidden diffraction spots (inset Figure in 3b) might be related to secondary reflection.

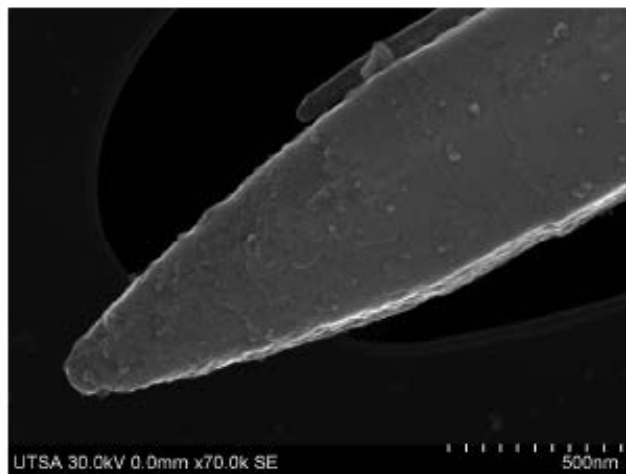


Figure 4. SEM image of the 5Ag/ZnO one dimensional catalyst.

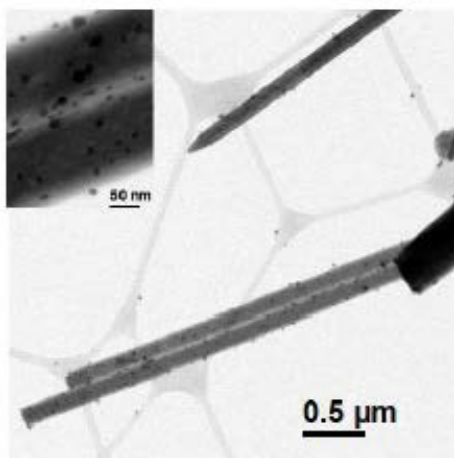


Fig.5. Low magnification TEM image of the 5Ag/ZnO 1D catalyst. Inset Figure showed the higher magnification of the one dimensional catalyst.

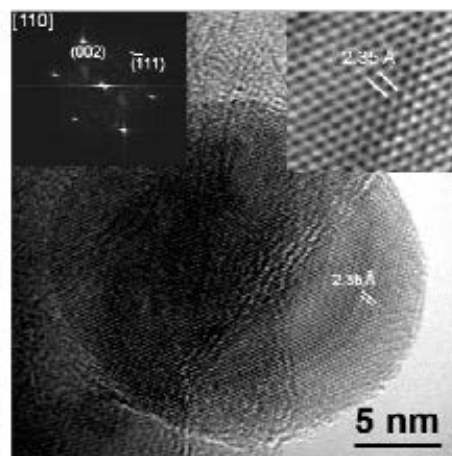


Fig. 6 Aberration corrected HRTEM image of a 5Ag/ZnO catalyst which was recorded along [110] orientation. The d-spacing measured between two adjacent planes of atoms was measured to be $\approx 2.35 \text{ \AA}$ corresponding to the {111} planes. The particle size was about 22.5 nm. The FFT is shown inset.

We used the ZnO 1-D rods for silver impregnation and tested as catalysts for catalytic applications. Figure 4 showed the SEM image of the 5Ag/ZnO 1-D catalyst. It is possible to observe spherical nanoparticles over the ZnO rods. In addition, the morphology of the ZnO rods was maintained after silver impregnation and thermal treatments. The size of the individual nanoparticles can extend up to 30 nm in diameter in accordance with the TEM images (Figure 5), in which we observed Ag nanoparticles with quasi-spherical morphology and average size about 15-30 nm (inset Figure) homogeneously distributed along the rods. The TEM images of the 5Ag/ZnO 1D catalyst showed good dispersion of the silver nanoparticles over the entire ZnO rod. Figure 6 shows the HRTEM image of silver nanoparticles deposited on the ZnO 1D rod, and was indexed assuming Fm-3m symmetry obtaining a unit cell value of 4.09 Å in agreement with the data reported for the JCPDS card number 065-2871. On the other hand, the nanoparticles showed lattice fringes with interplanar spacing of 0.235 nm corresponding to the {111} planes of fcc Ag. The Fast Fourier transform (FFT) pattern (inset in Figures) also confirms fcc metallic Ag along the [110] zone axis.

The surface area of the ZnO 1-D rods without any thermal treatments was 1 m²/g. Impregnation with 1.5 or 5 wt. % of silver to ZnO 1-D rods, did not modified the value of the surface area of the samples. The crystalline structure of the ZnO, 1.5Ag/ZnO and 5Ag/ZnO catalysts powder was investigated by XRD and showed in Figure 7. The ZnO one dimensional rods showed well crystalline structure with a sharp diffraction peaks and corroborate our above observations with TEM technique. The ZnO structure corresponds to the typical Wurzite structure (hexagonal with space group P63mc corresponding to the JCPDS 36-1451). This indicates that even the samples

were synthesized at lower temperatures it had a well-defined crystalline structure. In addition, no diffraction peaks from Zn or other impurities have been found in this sample. After silver impregnation and thermal treatments, the XRD patterns of the 1.5Ag/ZnO and 5Ag/ZnO showed peaks corresponding to Ag⁰ (JCPDS 065-2871) and peaks of the ZnO structure. On the other hand, no diffraction peaks of the metallic Zn or intermetallic Zn-Ag were observed on the samples. However, these structures cannot be excluded on the surface of the catalysts. As well as, it could be observed that the peak identified as metallic Ag increase as a function of silver loading. The average crystal size of the Ag measured by Scherer equation was 28.3 nm and 33.3 nm for 1.5Ag/ZnO and 5Ag/ZnO catalysts respectively.

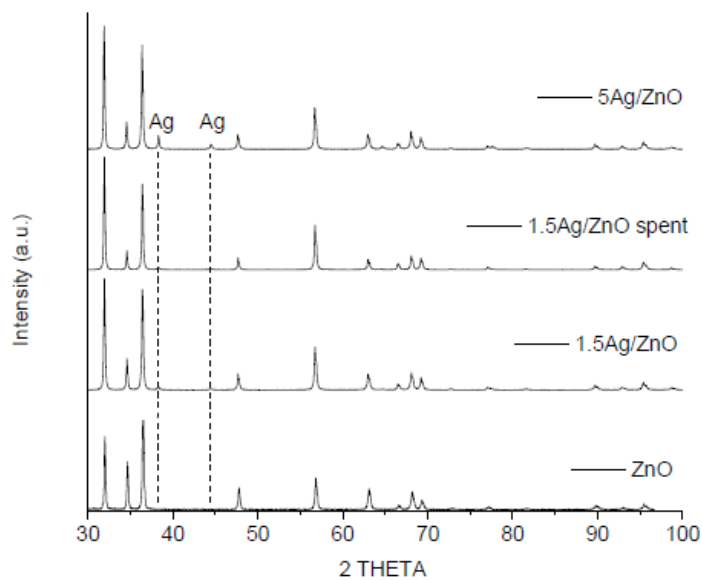


Figure 7. XRD pattern of the ZnO, 1.5Ag/ZnO 1D (fresh and spent) and 5Ag/ZnO 1D catalysts. ZnO wurzite structure and metallic silver.

The XRD pattern of the spent 1.5Ag/ZnO catalyst from the SRM reaction was characterized in order to determinate if the crystalline structure was maintained. Figure

7 showed that the 1.5Ag/ZnO one dimensional catalyst not suffer any change at the end of the reaction (second cycle). This finding suggests that the Ag/ZnO samples were very stable during the reaction. However, the average Ag particle size decreases after catalytic reaction until 21.6 nm. TPR profiles of the calcined samples and catalysts after catalytic reaction did not show a positive peak from r.t. to 500 °C, associated with the consumption of hydrogen necessary for the reduction of the silver oxide or some reducible species present on the catalyst (Figures not show). This result was attributed to that all the silver oxide probably is reduced at below ambient temperature.

Figure 8 showed the temperature dependence of the catalytic performance on methanol steam reforming over Ag/ZnO one dimensional catalysts from 225 to 400 °C. The catalytic performance of the steam reforming of methanol reaction of the bare ZnO showed tiny catalytic activity at low temperature but, when it was increased may display excellent SRM performance. Methanol conversion over the Ag-free ZnO support at 350 °C was 5 % and at 400 °C was 64 %.

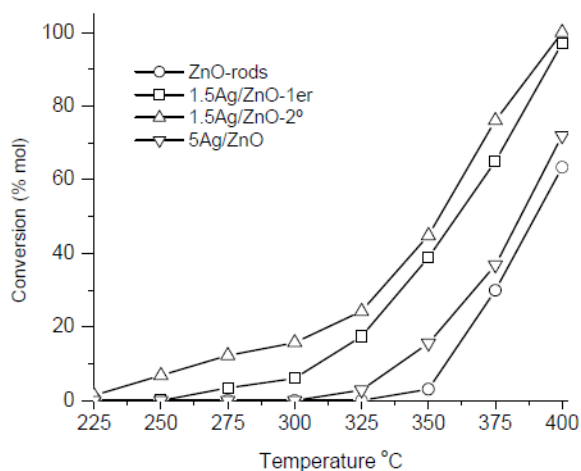


Figure 8. Temperature dependence of SRM activity of the Ag/ZnO one dimensional catalysts. Partial pressure of CH₃OH and H₂O was 75 and 12.75 Torr respectively. GHVS=30,000 h⁻¹. H₂O/CH₃OH = 1.0 mole ratio.

Koga et al. [34] studied the auto thermal reforming of methanol reaction on ZnO whiskers. They showed that the ZnO whiskers used in their study did not present any catalytic activity towards the methanol reforming reaction. However, when Cu was deposited on it, methanol conversion was observed at 250 °C. Mo et al. [35] studied the POM reaction over different CeO₂ and ZnO powders. They observed 85 % of the methanol conversion on CeO₂ synthesized in their laboratory and 0 % for commercial CeO₂ and ZnO respectively. On the other hand, when 1.5 wt. % of silver was supported on the ZnO 1D, the sample showed better performance on the steam reforming of methanol reaction than bare ZnO 1D. The light-off temperature for the 1.5Ag/ZnO 1D sample was approximately at 275 °C while on the 5Ag/ZnO 1D sample it was near to 300 °C. The methanol conversion at 350 °C was ~ 39 and ~ 16 % for 1.5Ag/ZnO and 5Ag/ZnO one dimensional catalysts respectively. The catalytic activity of the samples at the maximum reaction temperature showed the following order: 1.5Ag/ZnO > 5Ag/ZnO > ZnO 1D samples. This finding could be correlated with the Ag particle size present on the samples. The catalyst with small Ag particle size showed high catalytic activity than sample with big Ag particle size. Croy et al. [36] studied the H₂ production through methanol decomposition on Pt/TiO₂ catalysts. They observed high catalytic activity on the catalysts with small particle size and diminish as the particle size increase. On methane combustion was observed better catalytic activity on the catalyst with low gold loading than the one with high gold loading, this result was associated with the dispersion of Au and the atomic ratio of Au³⁺/Au⁰ [37; 38]. On the other hand, the catalyst that showed best performance in the catalytic activity was evaluated on a second cycle of the reaction, and it was found that the overall activity was slightly higher

than the first cycle of the reaction. This finding could be associated at the particle size as was reported on XRD section for this sample.

The main products of the SRM reaction over the Ag/ZnO 1D catalysts were H₂, CO and CO₂; among them; H₂ and CO₂ were the principal products. At the beginning of the reaction where tiny methanol is consumed only CO₂ and H₂O were produce. Figure 9a showed the H₂ yield (μmol) as a function of temperature on the SRM reaction of the ZnO, 1.5Ag/ZnO and 5Ag/ZnO 1-D catalysts. Between them, the 1.5Ag/ZnO one dimensional sample had the best H₂ yield than ZnO and 5Ag/ZnO 1D samples. The H₂ yield observed on the 1.5Ag/ZnO 1D sample was 2.48 μmole at 400 °C but on the second cycle of the reaction the value increase until 2.73 (the theoretical value for SRM is 3). On the other hand, it is cleared that the H₂ production on the first and second cycle of the reaction of the 1.5Ag/ZnO 1D catalyst was practically the same in whole reaction temperature. Bare ZnO and 5Ag/ZnO one dimensional samples showed approximately the same H₂ production, between them the last sample had lowest selectivity toward hydrogen. It is interesting to notice that the CO production during the entire process is near to 0.1 μmol at the maximum reaction temperature 9b. While, the main carbon product from the SRM reaction was CO₂. At 400 °C in which almost all methanol was consumed, the final products were H₂, H₂O, CO and CO₂. It is well known [39; 40; 41] that on the pd/ZnO catalysts selectively catalyzes the formation of H₂/CO₂ virtually free of CO; this finding was attributed at the Pd/Zn alloy formed on those catalysts. Koga et al. [34] attributed the low CO production to the arrangement between Cu/ZnO whiskers embedded in a paper composite rather than the catalysts. Mo et al. [35] observed 51 and 13 % of CO selectivity for CeO₂ and CeO₂(20%)ZnO catalysts

respectively. Bianchi et al. [42] observed bifunctional effect between the active phase and the support during methanol decomposition, where zirconia provides adsorption sites for reaction intermediates and Cu is proposed to facilitate the transfer and utilization of hydrogen. Similar results were reported by Bell [43] and Agrell [44]. This phenomenon could be occurring in our Ag/ZnO one dimensional catalyst. In this case the high Zn/Ag ratio favors the possible silver-support interaction, increasing the bifunctional role between the active phase and the ZnO edge sites beneficial for the reaction; in addition ZnO avoids the formation of CO. However, high loading of silver nanoparticles can reduce the surface active for the catalytic reaction dropping the reaction, as was observed on the 5Ag/ZnO one dimensional catalyst. Because, high content of Ag on the rods diminish the methanol adsorption over zinc oxide and hence avoid the dissociative adsorption of methanol. Those reports and our results of the catalytic activity, suggest that the base-ZnO samples could be suppressed the undesirable CO byproduction. This is known to act as a catalytic poison for Pt anode electrocatalysts in fuel cells.

The main products of the SRM reaction of the Ag/ZnO 1D catalysts were H₂, CO and CO₂; among them; H₂ and CO₂ were the principal products. At the beginning of the reaction where tiny methanol is consumed only CO₂ and H₂O were produce. Figure 9a showed the H₂ yield (μmol) as a function of temperature on the SRM reaction of the ZnO, 1.5Ag/ZnO and 5Ag/ZnO 1-D catalysts. Between them, the 1.5Ag/ZnO one dimensional sample had the best H₂ yield than ZnO and 5Ag/ZnO 1D samples.

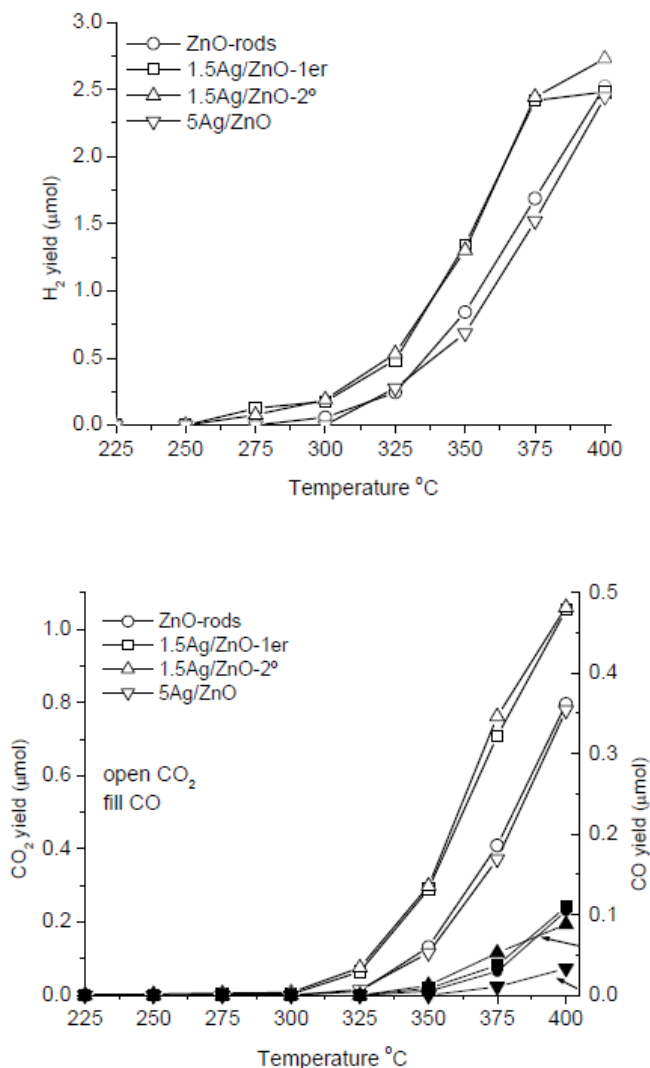


Figure 9. a) H₂ yield, b) CO₂ (thick line) and CO (thin line) yield as a function of the reaction temperature. Partial pressure of CH₃OH and H₂O was 75 and 12.75 Torr respectively. GHVS=30,000 h⁻¹. H₂O/CH₃OH = 1.0 mole ratio.

The H₂ yield observed on the 1.5Ag/ZnO 1D sample was 2.48 μmole at 400 °C but on the second cycle of the reaction the value increase until 2.73 (the theoretical value for SRM is 3). On the other hand, it is cleared that the H₂ production on the first and second cycle of the reaction of the 1.5Ag/ZnO 1D catalyst was practically the same in whole reaction temperature. Bare ZnO and 5Ag/ZnO one dimensional samples showed approximately the same H₂ production, between them the last sample had

lowest selectivity toward hydrogen. It is interesting to notice that the CO production during the entire process is near to 0.1 μmol at the maximum reaction temperature 9b. While, the main carbon product from the SRM reaction was CO_2 . At 400 $^\circ\text{C}$ in which almost all methanol was consumed, the final products were H_2 , H_2O , CO and CO_2 . It is well known [39, 40, 41] that on the Pd/ZnO catalysts selectively catalyzes the formation of H_2/CO_2 virtually free of CO; this finding was attributed at the Pd/Zn alloy formed on those catalysts. Koga et al. [34] attributed the low CO production to the arrangement between Cu/ZnO whiskers embedded in a paper composite rather than the catalysts. Mo et al. [35] observed 51 and 13 % of CO selectivity for CeO_2 and $\text{CeO}_2(20\%)\text{ZnO}$ catalysts respectively. Bianchi et al. [42] observed bifunctional effect between the active phase and the support during methanol decomposition, where zirconia provides adsorption sites for reaction intermediates and Cu is proposed to facilitate the transfer and utilization of hydrogen. Similar results were reported by Bell [43] and Agrell [44].

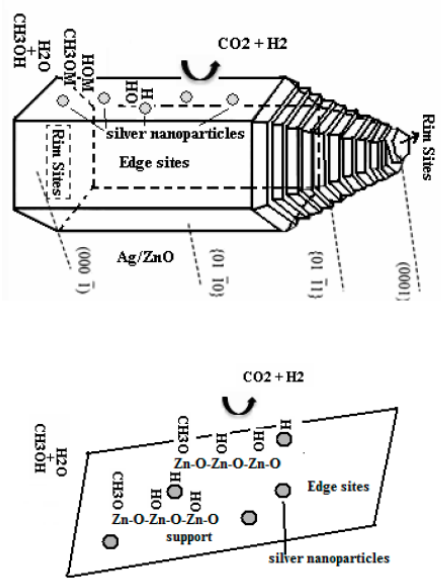
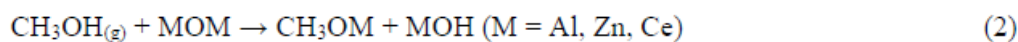


Figure 10. Rim and edge sites for Ag/ZnO one dimensional catalyst and reaction mechanism from eq. 2-5.

This phenomenon could be occurring in our Ag/ZnO one dimensional catalyst. In this case the high Zn/Ag ratio favors the possible silver-support interaction, increasing the bifunctional role between the active phase and the ZnO edge sites beneficial for the reaction; in addition ZnO avoids the formation of CO. However, high loading of silver nanoparticles can reduce the surface active for the catalytic reaction dropping the reaction, as was observed on the 5Ag/ZnO one dimensional catalyst. Because, high content of Ag on the rods diminish the methanol adsorption over zinc oxide and hence avoid the dissociative adsorption of methanol. Those reports and our results of the catalytic activity, suggest that the base-ZnO samples could be suppressed the undesirable CO byproduction. This is known to act as a catalytic poison for Pt anode electrocatalysts in fuel cells.

According to the SEM and TEM results we propose that the edge sites are responsible of the catalytic reaction than the flat basal planes (rim sites). In other words, we suggest that the low rim/edges sites ratio of the ZnO rods is responsible for the catalytic activity and selectivity toward H₂ and low CO production, because, rods have larger edge area for the catalytic reaction than rim sites (Figure 10). We suggests that the next steps (2-5) could be occur on the edges sites of our Ag/ZnO one dimensional catalyst via the Mars and van Krevelen (MVK) mechanism then the role of Ag is to accept the hydrogen to be released to the gas phase (Figure 10) as Cu-base catalysts previously reported [7].



Conclusions

The ZnO 3D nanostars and 1D-crystalline ZnO rod arrays has been growth by hydrothermal method. The ZnO 1D rods were impregnated with silver by the classic impregnation technique. SEM and TEM results showed that is possible to prepare good silver nanoparticles dispersed over entire surface of the ZnO 1D rods. The average Ag crystallite size determined by Scherrer equation in DRX analysis was 28.3 nm for the 1.5Ag/ZnO sample and 33.3 nm for the 5Ag/ZnO catalysts respectively. These Ag/ZnO 1D rods catalysts showed good catalytic activity on the steam reforming methanol reaction for hydrogen production. Among these catalysts, the sample with small Ag particle size showed best performance in methanol conversion than on the catalyst with big Ag particle size. Good stability during the reaction was observed on the 1.5Ag/ZnO 1D sample (second cycle of reaction). According to the results of SEM and TEM techniques the catalytic activity observed on the ZnO one dimensional catalyst occurs in the edge sites rather than in the rim sites. The high ZnO/Ag ratio from the edge sites is responsible of the high catalytic activity and selectivity toward H₂ and low CO production. In addition, the H₂ yield reaches the value of 2.48 in the first cycle of the reaction and increase up to 2.78 in the second cycle of the reaction at 400 °C which is very close to the theoretical one. On the other hand, the controllable growth of ZnO nanostructures described here may open up the possibility of exploring novel applications in the areas of catalysis in addition to high volume applications.

Acknowledgements

The authors are indebted to the Welch foundation through grant funding, Peñoles Company in Mexico and the projects ININ-CA-711, ININ-CA-009 and CONACyT

(México) J-48924 for financial support. Thanks to D. Olmos MSc and Dr. D. Ferrer for their technical support.

References

- [1] A.A. Mirzaei, H.R. Shaterian, S.H. Taylor, G.J. Hutchings: *Catal. Letters* Vol. 87 (2003), p. 103.
- [2] B. Lindstrom, L.J. Pettersson: *Int J Hydrogen Energy* Vol. 26 (2001), p. 923.
- [3] L.J. Pettersson, R. Westerholm: *Int J Hydrogen Energy* Vol. 26 (2001), p. 243.
- [4] R. Perez-Hernandez, G. Mondragon-Galicia, D. Mendoza-Anaya, J. Palacios, C. Angeles-Chavez, J. Arenas-Alatorre: *Int J Hydrogen Energy* Vol. 33 (2008), p. 4569.
- [5] R. Perez-Hernandez, A. Gutierrez-Martinez, C.E. Gutierrez-Wing: *Int J Hydrogen Energy* Vol. 32 (2007), p. 2888.
- [6] M. Turco, C. Cammarano, G. Bagnasco, E. Moretti, L. Storaro, A. Talon, M. Lenarda: *Appl. Catal. B: Env.* Vol. 91 (2009), p. 101.
- [7] M. Turco, G. Bagnasco, C. Cammarano, P. Senese, U. Costantino, M. Sisani: *Appl. Catal. B: Env.* Vol. 77 (2007), p. 46.
- [8] S. Fukahori, T. Kitaoka, A. Tomoda, R. Suzuki, H. Wariishi: *Appl. Catal. A: Gen.* Vol. 300 (2006), p. 155.
- [9] T.L. Reitz, S. Ahmed, M. Krumpelt, R. Kumar, H.H. Kung: *J. Mol. Catal. A: Chem.* Vol. 162

(2000), p. 275.

[10] T.L. Reitz, P.L. Lee, K.F. Czaplewski, J.C. Lang, K.E. Popp, H.H. Kung, J. Catal. Vol. 199

(2001), p. 193.

[11] R. Perez-Hernandez, L.C. Longoria, J. Palacios, M.M. Aguila, V. Rodriguez, Energy Materials 3 (2008), p. 152.

[12] N. Iwasa, T. Mayanagi, N. Ongawa, K. Sakata, N. Takezawa: Catal. Lett. Vol. 54 (1998),
p. 119.

[13] J. Strunk, K. Kahler, X. Xia, M. Comitti, F. Schuth, T. Reinecke, M. Muhle, Appl. Catal. A:

Gen. Vol. 359 (2009), p. 121.

[14] H. Sakurai, M.H.: Catal. Today Vol. 29 (1996), p. 361.

[15] H. Sakurai, M. Haruta: Appl. Catal. A: Gen. Vol. 127 (1995), p. 93.

[16] M.S. Spencer: Catal. Lett. Vol. 66 (2000), p. 255.

[17] W. Lu, G. Liu, S. Gao, S. Xing, J. Wang: Nanotechnology Vol. 19 (2008), p. 445711.

[18] E.P. Melian, O.G. Diaz, J.M.D. Rodriguez, G. Colon, J. Arana, J.H. Melian, J.A. Navio,

J.P. Pena: Appl. Catal. A: Gen. Vol. 364 (2009), p. 174.

[19] E. De La Rosa, S. Sepulveda-Guzman, B. Reeja-Jayan, A. Torres, P. Salas, N. Elizondo,

M. Jose-Yacaman: J. Phys. Chem. C Vol. 111 (2007), p. 8489.

[20] B. Reeja-Jayan, E. De la Rosa, S. Sepulveda-Guzman, R.A. Rodriguez, M.J.

Yacaman:

J. Phys. Chem. C Vol. 112 (2008), p. 240.

[21] S. Sepulveda-Guzman, B. Reeja-Jayan, E.d.l. Rosa, A. Torres-Castro, V.

Gonzalez-Gonzalez,

M. Jose-Yacaman: Mater. Chem. Phys. Vol. 115 (2009), p. 172.

[22] J.P. Perdew, Y. Wang: Phys. Rev. B. Vol. 45 (1992), p. 13244.

[23] M.E. Fernandez, C.Angeles-Ch, G. Mondragon-Galicia, V. Rodriguez-Lugo: J. Mat.

Sci.:

Materials in Medicine Vol. 15 (2004), p. 1.

[24] R. Perez-Hernandez, D. Mendoza-Anaya, M.E. Fernandez, A. Gomez-Cortes: J.

Mol Catal A:

Chemical Vol. 281 (2008), p. 200.

[25] R. Perez-Hernandez, F. Aguilar, A.Gomes-Cortes, G. Diaz, Catal. Today Vol. 107-108 (2005),

p. 175.

[26] R. Perez-Hernandez, A. Gomez-Cortes, J. Arenas-Alatorre, S. Rojas, R. Mariscal,

J.L.G. Fierro, G. Diaz: Catal. Today Vol. 107-108 (2005), p. 149.

[27] C. Gutierrez-Wing, R. Perez-Hernandez, G. Mondragon-Galicia, G. Villa-Sanchez,

M.E. Fernandez-Garcia, J. Arenas-Alatorre, D. Mendoza-Anaya: Solid State Sci. Vol. 11 (2009), p. 1722.

[28] L. Feng, J. Liu, J. She, N. Xu, S. Deng, J. Chen: J. Cryst. Growth Vol. 311 (2009),

p. 1435.

- [29] X. Gao, X. Li, W. Yu, Flowerlike: *J. Phys. Chem. Vol. B* 109 (2005), p. 1155.
- [30] Z.L. Wang: *J. Phys.: Condens. Matter Vol.* 16 (2004), p. R829.
- [31] T. Trinidad, J.D.P. DeJesus, P. O'Brien: *J. Mater. Chem. Vol.* 4 (1994), p. 1611.
- [32] W.J. Li, E.W. Shi, W.Z. Zhong, Z.W. Yin: *J. Cryst. Growth Vol.* 203 (1999), p. 186.
- [33] Z. Zhang, J. Mu, *J. Colloid Interface Sci. Vol.* 307 (2007), p. 79.
- [34] H. Koga, T. Kitaoka, H. Wariishi: *Chem. Commun. Vol.* 43 (2008), p. 5616.
- [35] L. Mo, X. Zheng, C.-T. Yeh: *Chem Phys Chem Vol.* 6 (2005), p. 1470.
- [36] J.R. Croy, S. Mostafa, J. Liu, Y.-H. Sohn, B.R. Cuenya: *Catal. Lett. Vol.* 118 (2007), p. 1.
- [37] Y. Zhang, J. Deng, L. Zhang, W. Qiu, H. Dai, H. He, *Catal. Today* 139 (2008) 29.
- [38] X. Zhang, H. Shi, B.Q. Xu, *Catal. Today Vol.* 122 (2007), p. 330.
- [39] S.T. Liu, K. Takahashi, M. Ayabe, *Catal. Today Vol.* 87 (2003), p. 247.
- [40] S.T. Liu, K. Takahashi, K. Uematsu, M. Ayabe, *Appl. Catal. A: Gen. Vol.* 283 (2005), p. 125.
- [41] S.T. Liu, K. Takahashi, K. Fuchigami, K. Uematsu: *Catal. A: Gen. Vol.* 299 (2006), p. 58.
- [42] D. Bianchi, T. Chafik, M. Khalfallah, S.J. Teichner: *Appl. Catal. A Vol.* 123 (1995), p. 89.
- [43] I.A. Fisher, A.T. Bell, *J Catal. Vol.* 184 (1999), p. 357.
- [44] J. Agrell, H. Birgersson, M. Boutonnet, I. Melian-Cabreara, R.M. Navarro, J.L.G. Fierro: *J Catal Vol.* 219 (2003), p. 389.